Magnetic phase diagrams of the trilayers with the noncollinear coupling in the form of the proximity magnetism model

Shi-shen Yan[a] and P. Grünberg
Institut für Festkörperforschung, Forschungszentrum Jülich GmbH, D-52425 Jülich, Germany

Liang-mo Mei
Physics Department, Shandong University, Jinan, Shandong 250100, People's Republic of China

(Received 23 December 1999; accepted for publication 6 April 2000)

The magnetic phase diagrams of Fe/Mn/Fe trilayers with the noncollinear interlayer coupling in the form of the proximity magnetism model were theoretically studied. The C_+-C_- phase diagram in the remanent magnetization state predicts very rich spin configurations. The $H-C_+$ and $H-C_-$ phase diagrams show that the spin configurations of Fe/Mn/Fe trilayers depend strongly on the external magnetic field, the anisotropy of Fe layers, and the coupling coefficients C_+ and C_-. Our experimental results of noncollinear spin configurations of Fe/Mn/Fe trilayers strongly support the magnetic phase diagrams based on the proximity magnetism model. © *2000 American Institute of Physics.* [S0021-8979(00)00914-2]

I. INTRODUCTION

The magnetic phase diagrams of the layered magnetic structures have been greatly enriched owing to the antiferromagnetic (AF) interlayer coupling and noncollinear coupling, which were found in many magnetic layered structures, such as Fe/Cr/Fe,[1–3] Fe/(Al,Au)/Fe,[4] Fe/(Cu,Ag)/Fe,[5] Fe/Mn/Fe[6,7] trilayers and Fe/Cr multilayers.[8] Theoretically the magnetic phase diagrams strongly depend on the energy expression of the interlayer coupling. For the layered magnetic structures with nonmagnetic metallic interlayers, the interlayer coupling can be characterized by the following phenomenological energy expression:

$$E_c = -j_1 \cos(\theta) - j_2 \cos^2(\theta), \tag{1}$$

where θ is the angle between the magnetization vectors of the two ferromagnetic (FM) layers. Here the first term with the parameter j_1 represents the bilinear coupling which aligns the magnetic moments parallel if $j_1>0$ and antiparallel if $j_1<0$. The second term with j_2 describes the 90° coupling which creates a perpendicular alignment of the magnetic moments for $j_2<0$.

However, strictly speaking, Cr and Mn are not ''nonmagnetic'' metal spacers as often tacitly assumed. So another phenomenological model, i.e., the proximity magnetism model[9] was suggested by Slonczewski, which is based on the helicoidal quasi-AF ordering of the interlayers (such as Cr and Mn) in conjunction with the long-range lateral thickness fluctuation due to interfacial roughness. In this model the exchange coupling energy per unit area can be written as:

$$E_c = C_+(\theta)^2 + C_-(\theta-\pi)^2, \tag{2}$$

where $C_+ \geqslant 0$, $C_- \geqslant 0$, and $0 \leqslant \theta \leqslant \pi$. Here C_+ and C_- are the coupling coefficients, and θ as above is the angle between the magnetization vectors of the two FM layers. The origin of the simple square dependence is based on the assumption that the same tilt angle $\Delta\theta$ between the magnetization vectors of the nearest neighbor atomic planes of the interlayer away from the antialignment is only small and so higher terms in the series expansion of the coupling energy as a function of $\Delta\theta$ can be neglected. This translates to the same dependence on the angle θ between the magnetization vectors of the two FM layers as shown in Eq. (2). If neither C_+ nor C_- vanishes, the mutual equilibrium orientation of the two magnetizations in the FM layers is not collinear. But if one of the two coefficients C_+ and C_- vanishes for the perfect spacers (no thickness fluctuation), the equilibrium of the two magnetizations is collinear (AF or FM coupling). Comparable mixtures of even and odd monolayers of the spacers may give $C_+=C_-$, which constitutes an orthogonal coupling.

Up to now, based on the interlayer coupling energy in the form of Eq. (1) several authors have analyzed the spin configurations in the coupled multilayers[10–15] but few authors have done the work based on Eq. (2), whereas the proximity magnetism model has been successfully used to describe the very strong 90° coupling in CoFe/Mn/CoFe trilayers,[6] the 50° coupling in Fe/Cr multilayers,[8] and the trivial noncollinear coupling in Fe/Mn/Fe trilayers.[7] Experimentally the difference between Eqs. (1) and (2) shows up in a subtle difference concerning saturation after remagnetization. Though Eq. (1) implies full saturation of the $M-H$ curve at a finite critical external field, Eq. (2) implies an asymptotic approach toward saturation. Theoretically we can expect that the magnetic phase diagrams will be different owing to the different energy expressions of the interlayer coupling.

On the other hand, both Eqs. (1) and (2) predict very rich spin configurations in the remanent magnetization states, but

[a]Author to whom correspondence should be addressed; present address: Center for Materials for Information Technology, The University of Alabama, Tuscaloosa, AL 35487-0209; electronic mail: syan@mint.ua.edu

only a few spin configurations have been experimentally found, such as FM coupling, AF coupling,[1] 90° coupling,[2–6] 135° coupling in FeNi/Ag multilayers,[16] and 50° coupling in Fe/Cr multilayers.[8] Only recently, trivial noncollinear coupling states were found in Fe/Mn/Fe (Ref. 7) and Fe/Cr/Fe trilayers[3] and they seem to be a common phenomenon for samples with interfacial roughness. So it is necessary to give more experimental evidence for the noncollinear spin configurations to prove the theoretical predictions in the magnetic phase diagrams. In this article, we first report the theoretical magnetic phase diagrams of the magnetic trilayers with the noncollinear interlayer coupling in the form of the proximity magnetism model, and then we present some experimental results of noncollinear spin configurations of Fe/Mn/Fe trilayers to support our calculations based on the proximity magnetism model.

II. THEORETICAL MAGNETIC PHASE DIAGRAMS

As an example we calculate the magnetic phase diagrams of a real system like Fe/Mn/Fe or Fe/Cr/Fe trilayers with the following assumptions. In Fe/Mn/Fe trilayers the spins of Fe are assumed to lie parallel to the film plane, and so there is not a static demagnetizing field. We also assume that the spins within an individual Fe layer remain parallel to one another because of a strong intralayer-exchange coupling. The details of the actual magnetic structures of the Mn (or Cr) are not considered, but its contribution to the total energy is represented by the exchange energy in the form of Eq. (2). In our case, the sample plane is parallel to (001) crystallographic plane and the external field is along the in-plane easy axis ([100] direction or equivalent). Taking into account the cubic anisotropy energy of Fe, Zeeman energy, and interlayer coupling energy in the form of Eq. (2), we write the total energy E per unit area in the following form:

$$\begin{aligned} &E=E_a+E_h+E_c,\\ &E_a=Kt[(\sin 2\Phi_1)^2+(\sin 2\Phi_2)^2]/4,\\ &E_h=-HMt(\cos\Phi_1+\cos\Phi_2),\\ &E_c=C_+(|\Phi_1-\Phi_2|)^2+C_-(|\Phi_1-\Phi_2|-\pi)^2, \end{aligned} \tag{3}$$

where E_a is the anisotropy energy, E_h is the Zeeman energy, and E_c is the interlayer coupling energy of the proximity magnetism model.[9] Here t, M, K, and H are, respectively, the thickness of Fe layers, the saturation magnetization of Fe layers, the first-order cubic crystal anisotropy of Fe layers, and the external field; Φ_1 (or Φ_2) is the angle between the magnetization vector of the first (or second) Fe layer and the field direction; and C_+ and C_- are the coupling coefficients which are the only two adjustable independent constants in our calculation. $|\Phi_1-\Phi_2|=\theta(0\leqslant\theta\leqslant\pi)$ is the angle between the two magnetization vectors of the Fe layers at a given external field (we call it coupling angle).

The theoretical magnetization curves and magnetic phase diagrams are obtained by minimizing the total energy of Eq. (3) with respect to Φ_1 and Φ_2 at a given external field H for the appropriate C_+ and C_-. By fitting in this way the theoretical magnetization curves to the experimentally measured hysteresis loops, one can quantitatively determine the experimental values of coupling coefficients C_+ and C_-, and the coupling angle $\theta=|\Phi_1-\Phi_2|$ at any given external field.

For simplicity and in order not to lose universality, we allow $0\leqslant\Phi_1-\Phi_2\leqslant\pi$ in Eq. (3). The minimum total energy should satisfy the equations $\partial E/\partial\Phi_i=0$ $(i=1,2)$, i.e.,

$$\frac{\partial E}{\partial\Phi_1}=2C_+(\Phi_1-\Phi_2)+2C_-(\Phi_1-\Phi_2-\pi)+\frac{Kt}{2}\sin(4\Phi_1)+HMt\sin\Phi_1=0, \tag{4a}$$

$$\frac{\partial E}{\partial\Phi_2}=-2C_+(\Phi_1-\Phi_2)-2C_-(\Phi_1-\Phi_2-\pi)+\frac{Kt}{2}\sin(4\Phi_2)+HMt\sin\Phi_2=0, \tag{4b}$$

with the stability condition that all the eigenvalues of the matrix M defined by $M_{ij}=\partial^2E/\partial\Phi_i\partial\Phi_j$ should be positive, i.e.,

$$\begin{aligned} &\frac{\partial^2E}{\partial\Phi_1^2}\frac{\partial^2E}{\partial\Phi_2^2}-\left(\frac{\partial^2E}{\partial\Phi_1\partial\Phi_2}\right)^2\\ &=(2C_++2C_-+2Kt\cos(4\Phi_1)+HMt\cos\Phi_1)\\ &\quad\times(2C_++2C_-+2Kt\cos(4\Phi_2)+HMt\cos\Phi_2)\\ &\quad-(2C_++2C_-)^2>0. \end{aligned} \tag{5}$$

It is easy to find that there are two kinds of solutions which satisfy Eqs. (4) and (5): the symmetrical solution $\Phi_1=-\Phi_2$ (symmetrical phase, i.e., the two magnetizations are symmetrical with respect to the direction of the applied field) and the asymmetrical solution $\Phi_1\neq-\Phi_2$ (asymmetrical phase, i.e., the two magnetizations are asymmetrical with respect to the direction of the applied field). But it is difficult to give the analytical expressions of (Φ_1,Φ_2). So the boundaries of the phases and the magnetization curves are, in general, obtained numerically. In fact, Eqs. (4) and (5) sometimes have more than one set of solutions of (Φ_1,Φ_2) for a given field H owing to different local positions of the local minimum energy. In this case we should choose the set of solution of (Φ_1,Φ_2) which corresponds to the global minimum energy. Therefore, we directly compare the different values of $E(\Phi_1,\Phi_2)$ at a given field H for all sets of (Φ_1,Φ_2) to find the global minimum, and then get the solution (Φ_1,Φ_2) to construct the phase diagram and the magnetization curve.

However, for zero external field we can give the analytical solutions of the boundaries of the phase diagram according to Eqs. (3)–(5). The C_--C_+ phase diagram at zero field is shown in Fig. 1. We have known that there are two phases: the symmetrical and the asymmetrical. At zero field the boundaries of the two phases are two straight lines in C_--C_+ phase diagram, i.e., $C_--3C_+=0$ and $3C_--C_+=0$. The symmetrical phase can be divided into two subphases S_1 and S_2, as shown in Fig. 1. In the S_1 region $(C_--3C_+>0)$ the spin configuration of the two magnetizations is symmetrical with respect to the easy axes, and the

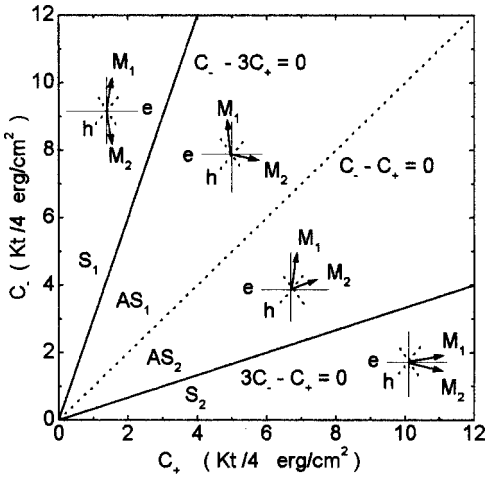

FIG. 1. The $C_- - C_+$ phase diagram at zero field. S and AS represent, respectively, the symmetrical and the asymmetrical configurations. The boundaries of the two phases (solid lines) are two straight lines, i.e., $C_- - 3C_+ = 0$ and $3C_- - C_+ = 0$. The dotted line is $C_- - C_+ = 0$. The insetted symbols show schematically the nonequal spin configurations of the two magnetizations in the Fe layers.

angle θ between the two magnetizations is in the range of $3\pi/4 < \theta \leqslant \pi$. Only when $C_+ = 0$ and $C_- > 0$, can the two magnetizations be aligned antiparallel (AF coupling). In the S_2 region ($3C_- - C_+ < 0$) the spin configuration is symmetrical, and the angle θ is in the range of $0 \leqslant \theta < \pi/4$. Only when $C_- = 0$ and $C_+ > 0$, can the two magnetizations be aligned parallel (FM coupling).

The asymmetrical phase can also be divided into two subphases AS_1 and AS_2, as shown in Fig. 1. In AS_1 region ($C_- - 3C_+ < 0$ and $C_- - C_+ \geqslant 0$) the spin configuration is asymmetrical with respect to the easy axes (but symmetrical with respect to the hard axes), and the angle θ is in the range of $\pi/2 \leqslant \theta < 3\pi/4$. Only when $C_+ = C_- > 0$, can the two magnetizations align perpendicularly (90° coupling). In the AS_2 region ($3C_- - C_+ > 0$ and $C_- - C_+ \leqslant 0$) the spin configuration is asymmetrical (but symmetrical with respect to the hard axes), and the angle θ is in the range of $\pi/4 < \theta \leqslant \pi/2$.

From the above we can see that the $C_- - C_+$ phase diagram at zero field is quite different from the $j_1 - j_2$ phase diagram (see Fig. 1 in Ref. 13). In $j_1 - j_2$ phase diagram there are wide regions of (j_1, j_2) where the two magnetizations are collinear (FM coupling phase I and AF coupling phase II in Fig. 1 of Ref. 13).

In Figs. 2(a)–2(d) we show the magnetic phase diagrams for different cases, where the external field is along the [100] direction of the easy axis. In our calculations we use the following typical experimental values of Fe layers: $M = 1707$ G s, $K = 4.76 \times 10^5$ erg/cm^3, and $t = 5 \times 10^{-7}$ cm. In Fig. 2(a) ($C_+ = 0$), the two magnetizations are always antiparallely aligned at zero field (AF coupling). For small but finite values of C_-, when the field is increased the system goes from the symmetrical configuration to the asymmetrical and then to the symmetrical again. For big but finite values of C_- the system is always symmetrical with respect to the applied field (the [100] direction of the easy axis).

In Fig. 2(b) ($C_+ = C_-$) the two magnetizations are always perpendicularly aligned at zero field (90° coupling). For any given $C_+ = C_- > 0$, the system goes from asymmetrical to symmetrical when the field is increased.

Figures 2(c) and 2(d) are two more universal cases. In Fig. 2(c) we show a $H - C_+$ phase diagram for fixed C_- ($C_- = 2.0\ Kt/4 = 0.1190$ erg/cm^2). For small but finite values of C_+, the system goes from the symmetrical configuration to the asymmetrical and then to the symmetrical again when the field is increased. For middle values of C_+, the spin configuration is asymmetrical at low field and become symmetrical at big field. For big but finite values of C_+ the system is always symmetrical.

In Fig. 2(d) we show the $H - C_-$ phase diagram for fixed C_+ ($C_+ = 2.0\ Kt/4 = 0.1190$ erg/cm^2). For small or big given

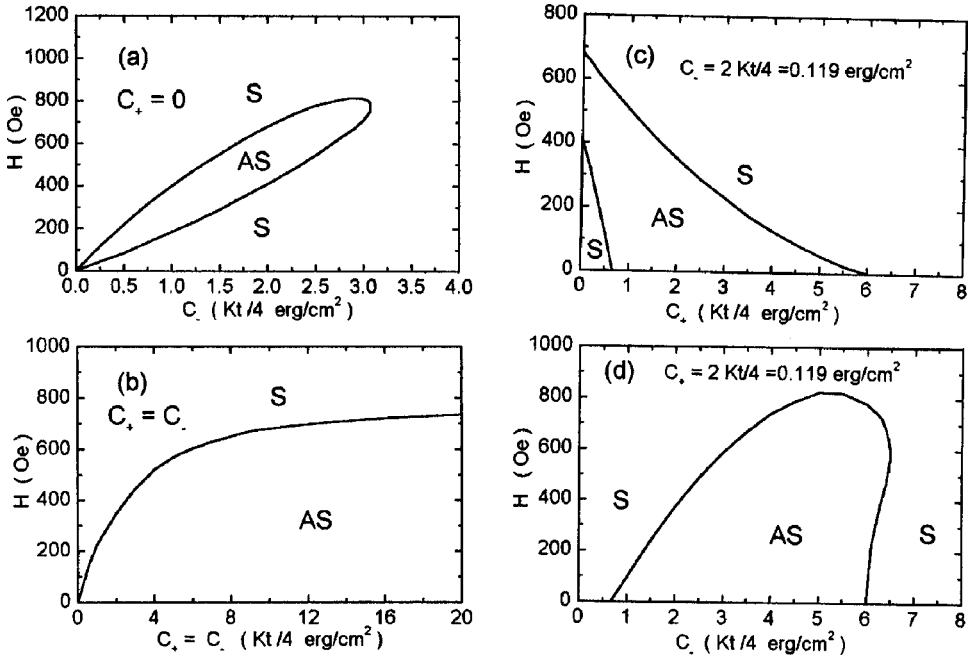

FIG. 2. The magnetic phase diagrams for different cases: (a) $H - C_-$ phase diagram for fixed $C_+ = 0$; (b) $H - C_+ = C_-$ phase diagram; (c) $H - C_+$ phase diagram for fixed $C_- = 2\ Kt/4 = 0.119$ erg/cm^2; and (d) $H - C_-$ phase diagram for fixed $C_+ = 2.0\ Kt/4$. The external field is along the [100] direction of the easy axis.

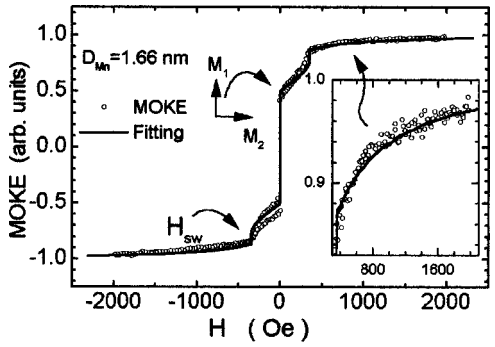

FIG. 3. The hysteresis loop measured by MOKE at room temperature (marked by circles) and the theoretical fitting by Eq. (3) (solid line). The Mn layer in this sample was deposited at 50 °C. The inset shows the details of the hysteresis loop in the high field range. The thickness of Mn layer D_{Mn} (nm), the coupling coefficients C_+ and C_- (erg/cm^2), and the coupling angle θ (deg) in remanence are, respectively, $D_{\mathrm{Mn}}=1.66$ nm, $C_+=C_-=0.118$ erg/cm^2, and $\theta=90°$.

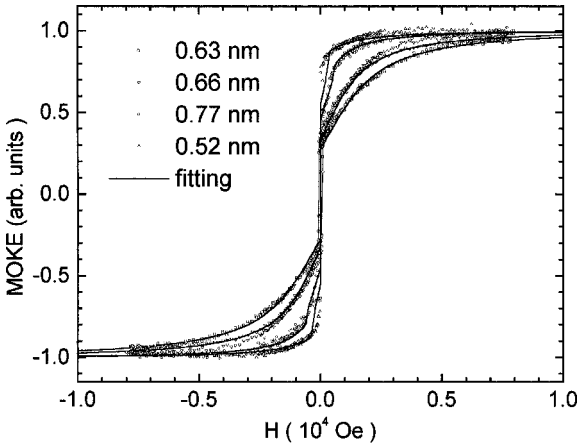

FIG. 4. Some typical hysteresis loops measured by MOKE at room temperature (marked by various symbols) and the theoretical fittings by Eq. (3) (solid lines). For these samples the Mn layers were deposited at −150 °C. The thickness of Mn layer D_{Mn} (nm), the coupling coefficients C_+ and C_- (erg/cm^2), and the coupling angle θ (deg) in remanence, are respectively, (up triangles) $D_{\mathrm{Mn}}=0.52$, $C_+=0.27$, $C_-=0.19$, $\theta=78$; (rectangles) $D_{\mathrm{Mn}}=0.63$, $C_+=0.13$, $C_-=0.52$, $\theta=148.5$; (down triangles) $D_{\mathrm{Mn}}=0.66$, $C_+=0.133$, $C_-=0.405$, $\theta=141.6$; and (circles) $D_{\mathrm{Mn}}=0.77$, $C_+=0.16$, $C_-=0.215$, $\theta=100$.

values of C_-, the system is always symmetrical. But for middle values of C_-, the field dependence of spin configuration is complicated. If $(2/3)(Kt/4)<C_-\leqslant 6(Kt/4)$, the spin configuration goes from asymmetrical to symmetrical when the field is increased. If $6(Kt/4)<C_-<6.15(Kt/4)$, the spin configuration will experience symmetrical, asymmetrical, and symmetrical for a given C_- when the field is increased.

The phase transition induced by the external field in Fig. 2 is always of the first order.

By the way, our calculations above are not limited to the Fe/Mn/Fe or Fe/Cr/Fe trilayers. They are also appropriate for Fe/Mn or Fe/Cr multilayers with infinite bilayers when the coefficients C_+ and C_- in Eq. (3) are, respectively, replaced by the coefficients $2C_{+m}$ and $2C_{-m}$. Here C_{+m} and C_{-m} are the coupling coefficients in the mutilayers.

III. COMPARING WITH THE EXPERIMENTAL RESULTS

In this section, we present our experimental results of noncollinear spin configurations of Fe/Mn/Fe trilayers to support our calculations based on the proximity magnetism model. The Fe 5 nm/Mn 0–4 nm/Fe 5 nm trilayers were deposited in UHV by the MBE method on GaAs/Fe 1 nm/Ag 150 nm substrate–buffer system and covered by 50 nm ZnS layer. The bottom 5 nm Fe layer was grown on Ag buffer at room temperature for the first 4 ML and at 200 °C for the rest. We prepared the Mn layer with the growth rate of about 0.9 nm/min at different temperatures from −150 to 200 °C. The top 5 nm Fe layer was deposited at 200 °C. We measured hysteresis loops and examined the coupling by longitudinal magneto-optic Kerr effect (MOKE). The external field was applied along the [100] direction of the easy axis, and parallel to both the sample plane and the incidence plane of the laser. Other details of the experiments are the same as described elsewhere.[2,7,17,18]

One direct and simple way to examine the theoretical magnetic phase diagrams is to compare the experimental hysteresis loops with the theoretical fittings. In Figs. 3 and 4 we show some typical hysteresis loops measured by MOKE at room temperature and the theoretical fittings (solid lines) only by adjusting C_+ and C_- in Eq. (3) for different samples. In Fig. 3 the remanent magnetization of about half of the saturation value and the big jump at near zero field indicate that the individual magnetizations switch between different easy axes but the angle between them remains 90°. We can see that the theoretical fittings are in good agreement with the experimental hysteresis loops obtained by MOKE. Especially, the following characters of the hysteresis loops are well described by the proximity magnetism model: first, all the hysteresis loops show an asymptotic approach toward saturation; and second, there are some noncollinear coupling states as shown in Fig. 4 except for the well known 90° coupling as shown in Fig. 3. Our theoretical fittings to the experimental hysteresis loops indicate that the coupling angles in the remanent magnetization states are, respectively, 78°, 148°, 141.6°, and 100° when the Mn layer thicknesses are, respectively, 0.52, 0.63, 0.66, and 0.77 nm. Further details will be reported.

Figures 5(a) and 5(b) show the dependence of spin configurations on the external field. In Fig. 5(a) (the magnetization hysteresis loop marked by down-triangles has been shown in Fig. 4), the angle between the two magnetizations is 141.6° at zero field. When the external field is less than 373 Oe, the two magnetizations are symmetrical. When the field is in the range from 373 to 676 Oe, the two magnetizations are asymmetrical. When the field is bigger than 676 Oe, the two magnetization become symmetrical again and asymptotically approach the direction of the external field.

In Fig. 5(b) (the magnetization hysteresis loop has been shown in Fig. 3), the two magnetizations are perpendicular to each other at zero field. When the external field is less than 355 Oe (the switching field H_{SW} in Fig. 3), the two magnetizations are asymmetrical. When the field is bigger than 355 Oe, the two magnetizations are symmetrical and asymptoti-

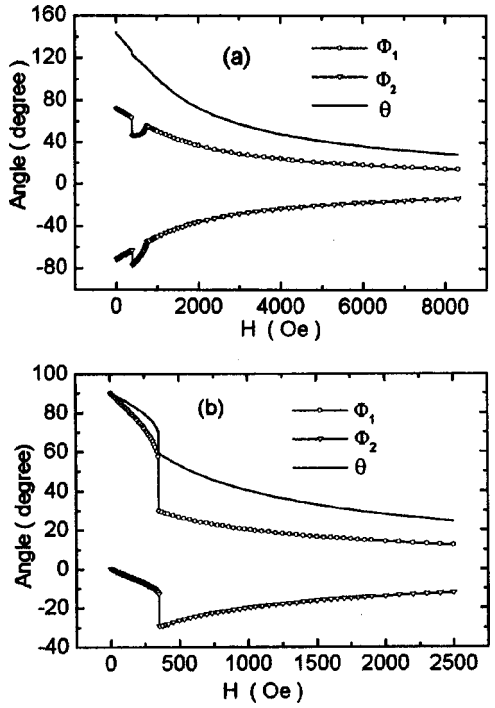

FIG. 5. The dependence of spin configurations on the external field. The line with circles (or triangles) represents angle Φ_1 (or Φ_2) between the magnetization of the first (or second) Fe layer and the external field; the solid line represents the angle θ between the two magnetizations: (a) $D_{\mathrm{Mn}}=0.66$ nm and (b) $D_{\mathrm{Mn}}=1.66$ nm.

cally approach the direction of the external field.

From the above experimental hysteresis loops of Fe/Mn/Fe trilayers, we can see that although the spin configurations and phase transitions induced by the external field seem to be complicated, they are quantitatively described by the proximity magnetism model. Physically, all possible spin configurations can be explained in accordance with the principle of minimum total energy in the Fe/Mn/Fe system [see Eq. (3)]. Approximately but simply speaking, in order to reduce the anisotropy energy and as a result reduce the total energy to the minimum, phase transitions occur. In fact, if there is no anisotropy, the spin configurations will always be symmetrical about the external field.

IV. CONCLUSIONS

In conclusion, the magnetic phase diagrams of Fe/Mn/Fe trilayers with noncollinear interlayer coupling in the form of the proximity magnetism model were theoretically studied. The C_+-C_- phase diagram in remnant magnetization states predicts very rich magnetic phases. The $H-C_+$ and $H-C_-$ phase diagrams show that the spin configurations of Fe/Mn/Fe trilayers depend strongly on the external field, the anisotropy of Fe layers, and the coupling coefficients C_+ and C_-. The above calculations based on the proximity magnetism model are strongly supported by our experimental results of noncollinear coupling in Fe/Mn/Fe trilayers.

From the viewpoint of theory, the good agreement between the experimental hysteresis loops of Fe/Mn/Fe trilayers and the theoretical calculations based on the proximity magnetism model suggests that the Fe/Cr/Fe system should be reexamined by the same idea since both Mn and Cr are antiferromagnetic materials. From the viewpoint of applications, the Fe/Mn/Fe trilayers supply a new artificial spin system where an arbitrary coupling angle in the ground state is available by modifying the interlayer thickness and growth conditions of the films, and where the switching of the magnetization vectors in the two Fe layers is easy to control by the external field. Since the giant magnetoresistance depends on the relative orientation of the magnetization vectors in the magnetic layers, the findings in this article may be useful in the design of magnetoresistive sensors.

ACKNOWLEDGMENTS

The authors thank R. Schreiber, F. Voges, D. Olligs, and P. Röttländ for their help. S.-s. Y. is pleased to thank the Alexander von Humboldt Foundation for support.

[1] P. Grünberg, R. Schreiber, Y. Pang, M. B. Brodsky, and H. Sowers, Phys. Rev. Lett. **57**, 2442 (1986).
[2] M. Rührig, R. Schäfer, A. Hubert, R. Mosler, J. A. Wolf, S. Demokritov, and P. Grünberg, Phys. Status Solidi A **125**, 635 (1991).
[3] D. T. Pierce, J. Unguris, R. J. Celotta, and M. D. Stiles, J. Magn. Magn. Mater. **200**, 290 (1999).
[4] A. Fuss, S. Demokritov, P. Grünberg, and W. Zinn, J. Magn. Magn. Mater. **103**, L221 (1992).
[5] Z. Celinski, B. Heinrich, and J. F. Cochran, J. Magn. Magn. Mater. **145**, L1 (1995).
[6] M. E. Filipkowski, J. J. Krebs, G. A. Prinz, and C. J. Gutierrez, Phys. Rev. Lett. **75**, 1847 (1995).
[7] S.-s. Yan, R. Schreiber, F. Voges, C. Osthöver, and P. Grünberg, Phys. Rev. B **59**, R11641 (1999).
[8] A. Schreyer, J. F. Ankner, Th. Zeidler, H. Zabel, M. Schäfer, J. A. Wolf, P. Grünberg, and C. F. Majkrzak, Phys. Rev. B **52**, 16066 (1995).
[9] J. C. Slonczewski, J. Magn. Magn. Mater. **150**, 13 (1995).
[10] B. Dieny, J. P. Gavigan, and J. P. Rebouillat, J. Phys.: Condens. Matter **2**, 159 (1990).
[11] R. W. Wang, D. L. Mills, Eric E. Fullerton, J. E. Mattson, and S. D. Bader, Phys. Rev. Lett. **72**, 920 (1994).
[12] N. S. Almeida and D. L. Mills, Phys. Rev. B **52**, 13504 (1995).
[13] V. V. Kostyuchenko and A. K. Zvezdin, Phys. Rev. B **57**, 5951 (1998).
[14] F. C. Nörtemann, R. L. Stamps, A. S. Carrico, and R. E. Camley, Phys. Rev. B **46**, 10847 (1992).
[15] T. L. Fonseca and N. S. Almeida, Phys. Rev. B **57**, 76 (1998).
[16] B. Rodmacq, K. Dumesnil, P. Mangin, and M. Hennion, Phys. Rev. B **48**, 3556 (1993).
[17] J. A. Wolf, Q. Leng, R. Schreiber, P. Grünberg, and W. Zinn, J. Magn. Magn. Mater. **121**, 253 (1993).
[18] M. Schäfer, S. Demokritov, S. Müller-Pfeiffer, R. Schäfer, M. Schneider, and P. Grünberg, J. Appl. Phys. **77**, 6432 (1995).